P5.3 CHANNEL SELECTION FOR THE NEXT GENERATION GEOSTATIONARY ADVANCED BASELINE IMAGERS

Timothy J. Schmit
NOAA/NESDIS, Office of Research and Applications, Advanced Satellite Products Team (ASPT)
Madison, WI
Tim.j.Schmit@noaa.gov

W. P. Menzel
NOAA/NESDIS, Office of Research and Applications
Madison, WI
Paul.Menzel@noaa.gov

Justin Sieglaff
Cooperative Institute for Meteorological Satellite Studies (CIMSS)
University of Wisconsin-Madison
Madison, WI
Justin.Sieglaff@ssec.wisc.edu

James P. Nelson III
Cooperative Institute for Meteorological Satellite Studies (CIMSS)
University of Wisconsin-Madison
Madison, WI
Jim.Nelson@ssec.wisc.edu

Michael K. Griffin
MIT/LL (Massachusetts Institute of Technology/Lincoln Laboratory)
Lexington, MA
griffin@ll.mit.edu

James J. Gurka
NOAA/NESDIS, Office of Systems Development
Suitland, MD
James.Gurka@noaa.gov

1. INTRODUCTION

The Advanced Baseline Imager (ABI) is being designed for future Geostationary Operational Environmental Satellites (starting with GOES-R in 2012) (Gurka and Dittburner 2001). As with the current GOES Imager, this instrument will be used for a wide range of qualitative and quantitative weather and environmental applications. The ABI will be improved over the existing GOES Imager with more spectral bands, higher spatial resolution, faster imaging, and broader spectral coverage. The ABI will improve the spatial resolution from 4 to 2 km nominally for the infrared bands and 1 to 0.5 km for at least one visible band. There will be a five-fold increase of the coverage rate. The ABI expands the spectral band number to at least 12; five are

---

Corresponding author address: Timothy J. Schmit, 1225 West Dayton Street, Madison, WI 53706; email: Tim.J.Schmit@noaa.gov.

similar to the 0.6, 4, 11, and 12 µm windows and the 6.5 µm water vapor band on the current GOES-8/11 Imagers. For more information on the uses of the current GOES Imager, see Menzel and Purdom (1994) and Ellrod et al. (1998). The additional bands are a visible band at 0.86 µm for the detection of aerosols and vegetation; a near-infrared band at 1.38 µm to detect very thin cirrus clouds; a snow/cloud-discriminating 1.6 µm band; a mid-tropospheric 7.0 µm water vapor band to track atmospheric motions; an 8.5 µm band to detect volcanic dust clouds containing sulfuric acid aerosols and cloud phase; a 10.35 µm band to derive low-level moisture and cloud particle size; and a 13.3 µm band useful for determining cloud top heights and effective cloud amounts. There is interest in adding bands centered at 0.47 µm for aerosol detection and visibility estimation, at 7.4 µm for lower/mid-level flow and sulfuric acid aerosols, and at 9.6 µm for monitoring atmospheric total column ozone on space and time scales never before possible. Lastly, bands at 2.26 and 3.7 µm would be used for land characterization. daytime land/cloud properties, particle size, vegetation and cloud properties/screening, hot spot detection, and moisture determinations. Every product that is being produced from the current GOES Imager will be improved with data from the ABI. In addition, new products will be possible.

The seven proposed visible/near infrared bands are shown in Fig. 1 with a representative clear-sky radiance plot. Figure 2 shows the eleven remaining proposed bands in the infrared portion of the spectrum.

The channel selection for ABI is a balance of heritage with existing GOES bands (on the imager or sounder), consistency with bands on other satellites (both in geostationary and polar-orbits) and also considers information that will be available from the advanced high-spectral resolution sounder. Section 2 summarizes a select number of new and improved products possible with the GOES ABI. Section 3 briefly describes the uses for each of the "core" or proposed bands on the ABI.

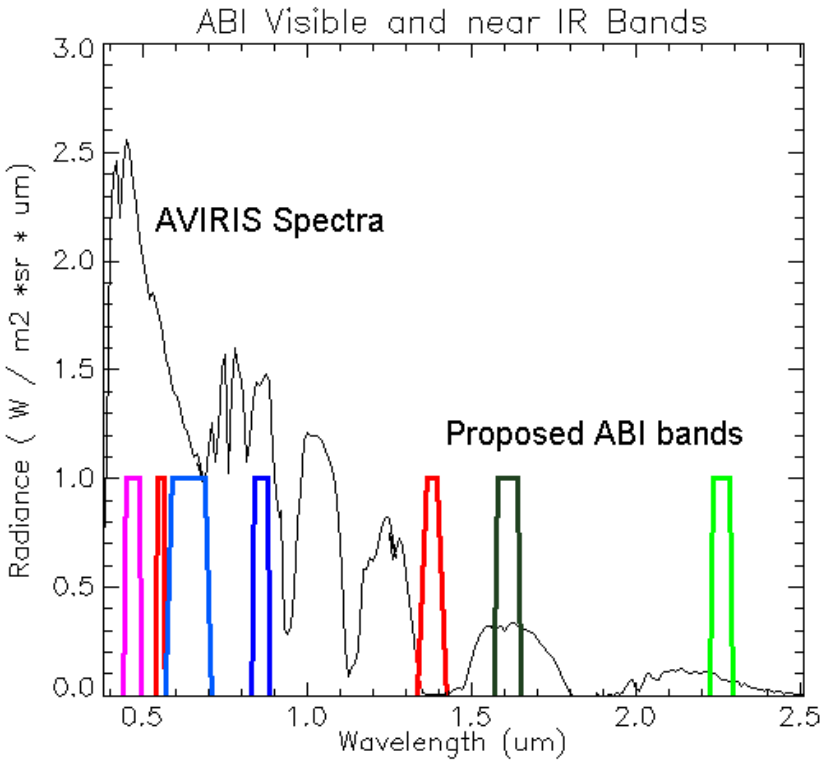

Fig. 1. The spectral coverage of the seven proposed visible/near infrared bands with a representative clear-sky radiance plot.

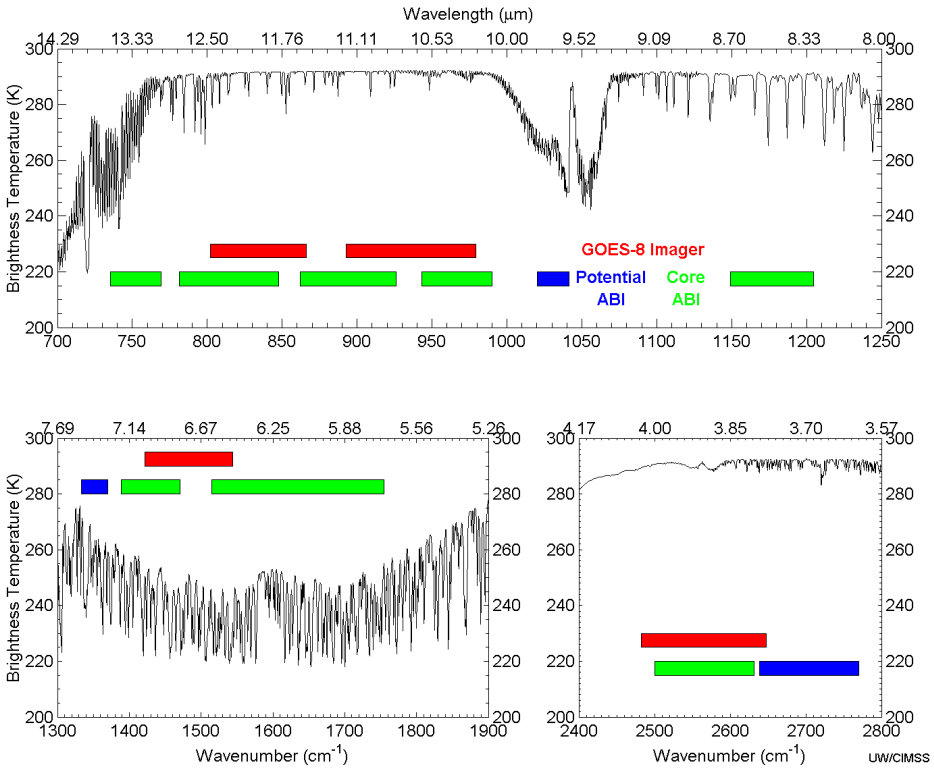

Fig. 2. The spectral coverage of the eleven proposed bands in the infrared portion of the spectrum.

2. PRODUCTS

2.1 Imagery/Radiances

Each of the current bands on the GOES Imager is displayed as a time-series of images. This will also be the case for each of the ABI bands. Additional information can be gleaned by computing differences between bands or applying principle component analysis on the imagery (Hillger 1996). For example, the current GOES Imager "water vapor" band 3 (6.7 μm) has many applications, ranging from estimating upper level moisture (Soden et al. 1993; Moody et al. 1999) to defining upper-level jetstreaks (Weldon et al. 1991). While the difference between the 11 and 12 μm brightness temperatures, known as the split window, helps detect dust, volcanic ash plumes, low-level moisture, and skin temperature and aids in distinguishing between cloud types and biomass burning aerosols (Ackerman 1996; Ackerman et al. 1992; Moeller et al. 1996; Prata, 1989; Barton et al. 1992; Hayden et al. 1996; Prins et al. 1998), outflow boundaries have also been observed (Dostalek et al. 1997). Also, averaged, clear-sky brightness temperatures from the imagers are being investigated for inclusion into numerical models. For example, the direct assimilation of water vapor (WV) clear-sky brightness temperatures (CSBT) from geostationary satellites became operational at ECMWF in April 2002 using the four-dimensional variational assimilation (4DVAR) system with data from METEOSAT-7. The GOES CSBT product will be improved with the ABI, in part due a superior cloud mask with the additional bands and a better signal-to-noise ratio.

2.2 Cloud Products

Cloud products generated via the CO_2 absorption technique have been demonstrated from instruments on both geostationary and polar-orbiting platforms (Wylie and Wang 1997; Schreiner et al. 1993; Wylie et al. 1994; Wylie and Menzel 1999; Frey et al. 1999; Schreiner et al. 2001). Cloud products derived from the GOES Sounder have been used to initialize numerical models (Kim et al. 2000; Bayler et al.

2001). Improved products from the GOES ABI will include cloud top pressure (CTP), effective cloud amount (ECA) and cloud top temperature. The ECA represents the optical thickness of the cloud. Recent work has shown that the difference between the 6.7 μm and the 11 μm bands is correlated to convection (Mosher 2001). These ABI cloud products will be improved over the current suite, especially if they are computed in conjunction with information from the Advanced Baseline Sounder (ABS) (Li et al. 2002).

2.3 Sea Surface Temperature (SST)

The GOES platform allows frequent looks at a given area with the same viewing angle. This scanning feature is exploited to generate spatial and temporal coverage of Sea Surface Temperature (SST) from the GOES Imager that is improved over what can be obtained from polar-orbiting satellites (Wu et al. 1999). The GOES SST products have many applications, ranging from weather forecasting to fishery management (Seki et al. 2001). The information used to create the SST product will be improved with the ABI due to: higher spatial resolution, more frequent images, better cloud and aerosol detection and less noisy data.

2.4 Dust and Volcanic ash detection

The detection of volcanic ash plumes is important for aviation applications (Casadevall et al. 1992; Davies and Rose 1998; Hillger and Clark 2001; Ellrod 2001). The ABI will improve volcanic ash detection by returning the 12 μm data to the imager (Schmit et al. 2001), but more importantly because it will include an 8.5 μm SO_2-sensitive band.

2.5 Rainfall estimations

Rainfall estimation techniques use data from the GOES Imager. Some rely on only the infrared window, for example the auto-estimator (Vicente et al. 1998), while others use more bands, such as the GOES Multispectral Rainfall Algorithm (GMSRA) (Ba et al. 2001). Both types of satellite rainfall estimations will be improved with the ABI data. This is due to the additional bands that will lead to a better cloud-type classification capability. Better spatial resolution and coverage rate will also improve rainfall estimates.

2.6 Satellite-derived wind fields

The tracking of atmospheric features (Velden et al. 1997) will be improved using the GOES ABI. The 13.3 μm data will provide better estimates of cloud height for the tracking of atmospheric motions. Currently, the height assignment is one of the greatest sources of error (Nieman et al. 1993). Satellite-derived winds will be improved with the ABI due to: higher spatial resolution (better edge detection), more frequent images (offering different time intervals), better cloud height detection (with multiple bands), new bands (0.86, 1.38 μm) that may allow wind products at different levels, better signal-to-noise ratio, and better image navigation/registration.

2.7 Objective Dvorak technique

The GOES Imager is currently used to determine hurricane location and intensity (Velden et al. 1998 a and b; Goerss et al. 1998; Bosart et al. 2000). The Objective Dvorak Technique is used to monitor the strength of tropical cyclones and relies on the longwave infrared window band (Velden et al. 1998a). The ABI, used in conjunction with the ABS, will allow a multi-spectral approach that will be investigated further. This product will also be enhanced due to the improved ABI temporal and spatial resolutions.

2.8 Biomass burning/smoke

The detection of active fires using primarily the 3.9 μm and the 11 μm bands (Prins et al. 1998) will be improved with the ABI. This is due in part to the improved spatial and temporal resolutions, along with the hotter maximum temperature allowed for the 3.9 μm band. The 0.47 μm band will also detect daytime smoke.

2.9 Fog detection

The bispectral technique for fog detection (Ellrod et al. 1998) is based on differences of the longwave and shortwave IR window brightness temperatures. Using simulated ABI data (derived from 1 km MODerate-resolution Imaging Spectroradiometer (MODIS) data), it has been shown that the fog detection capabilities of ABI will be an improvement over the current GOES Imager.

2.10 Aircraft icing

GOES Imagery is used to generate an experimental product that highlights areas of supercooled water clouds that could produce aircraft icing (Ellrod 1996). This product uses a split window (band 4 minus band 5) temperature difference of greater than 2 K to flag thin cirrus. The addition of the 1.6 and 8.5 μm bands should improve this product.

3. INDIVIDUAL BANDS OF THE PROPOSED ABI

3.1 0.47 μm or "blue" band

The utility of a band centered at 0.47 μm is well established from many satellites in low-earth orbit, including LANDSAT, SEAWIFS, MODIS and the future VIIRS on NPOESS. A geosynchronous platform is complementary to polar-orbiting platforms, providing otherwise unknown time-of-day and bi-reflectance data at mesoscale resolution. Blue-band radiances from GOES-R would provide nearly continuous observations of clouds, dust, haze and smoke, and would allow monitoring of the health of open waters.

The blue channel would be particularly valuable for aviation applications. The shorter wavelengths (blue) scatter more off haze and air particles than do the longer wavelengths (red). The current GOES visible channel frequency centered in the red was chosen to minimize scattering by haze in order to see the ground more clearly. Having an additional channel centered near the blue frequencies would greatly improve the detection of haze and enable calculations of slant range visibility. This channel would also have potential applications for air pollution studies, and for improving numerous other products that rely on obtaining clear sky radiances during the day (e.g., land and sea surface products).

3.2 0.555 μm or "green" band

The addition of a green (0.555 μm) band, along with the blue (0.47 μm) and red (0.64 μm) bands, would provide the meteorologists and the tax-paying public with true-color imagery of the atmosphere and its real time effects on land and sea. True color images readily show haze, smoke, snow, etc. This band, in conjunction with others, should also help monitor suspended sediment in bodies of water.

3.3 0.64 μm or "red" band

A very similar band already exists on the current GOES Imager. It has many uses, including the diurnal aspects of daytime clouds, fog detection and solar insolation (Diak et al. 1998). The 0.64 μm visible band is also used for: daytime snow and ice cover; detection of severe weather onset; low-level cloud drift winds; fog; smoke; volcanic ash, hurricane analysis; and winter storm analysis. Along with the 0.86 μm band, an NDVI (Normalized Difference Vegetation Index) could be generated.

3.4 0.86 μm

The 0.86 μm band is similar to a band on the next generation METEOSAT and would provide synergy with the AVHRR/3. This band is used for daytime clouds, NDVI, fog, aerosols and ocean studies. It can also help in determining vegetation amount and aerosol locations, and can be utilized for ocean/land studies. The band enables evaluation of localized vegetation stress and fire danger, fire burn scars and albedo retrieval, and may be useful for forecasting forest re-growth patterns. The current GOES visible channel (0.52 - 0.72 μm) does not delineate burn scars. Other applications include suspended sediment detection (Aquirre-Gomez 2000). Low-level winds may also be derived from time sequences of 0.86 μm images.

3.5 1.38 μm

The 1.38 μm band will help to detect thin cirrus clouds during the day. This is so because the band does not sense into the lower troposphere due to water vapor absorption and thus it provides excellent daytime sensitivity to thin cirrus. (The 1.38 μm band is centered *within* the atmospheric water vapor absorption region.) These thin clouds may not be detected with any other bands. Contrail detection is important to the climate change community and when estimating many surface parameters. When the Total Precipitable Water (TPW) value is too dry (for example, less than approximately 10 mm), then reflectance from the surface minimizes the benefits of this band for thin cirrus detection.

3.6 1.61 μm

During the day, the 1.6 μm band can be used for: cloud/snow/ice discrimination; total cloud cover; aviation weather analyses for cloud-top phase (Hutchison 1999); and detecting smoke from low-burn-rate fires. The 1.6 μm band displays a significant difference between the imaginary refractive index components for water and ice, which lends itself to cloud phase discrimination (Baum et al. 2000). Daytime water/ice cloud delineation is useful for aircraft routing.

3.7 2.26 μm

The 2.3 μm band is used mainly for cloud particle size determination. Particle growth is an indication of cloud growth and intensity of that growth. Other uses of the 2.26 μm band include cloud screening, hot spot detection, and total moisture determinations. For example, the MODIS cloud mask algorithm employs a very similar band (Ackerman et al. 1998). This band is being considered for the next generation European imager. The 2.26 μm band is also very useful to characterize the "aerosol-free" surface reflectance, so aerosols over land can then be characterized by the visible bands.

3.8 3.7 μm

The 3.7 μm band can be used for daytime land/cloud properties, particle size, night-time surface temperatures and possibly vegetation estimates. It can also be used, along with the 3.90 μm band, to estimate the amount of solar radiation. This band may help with "snow age" calculation and is also included on the MODIS instrument (Li et al. 2002).

3.9 3.90 μm

The shortwave IR window (3.9 μm) band has many uses: fog (Ellrod et al. 1998) and low-cloud discrimination at night; fire identification (Prins et al. 1998); volcanic eruption and ash detection; and daytime reflectivity for snow/ice. This band is based on the current GOES Imager band 2.

3.10 6.15 μm

Based on current GOES and the MSG/ SEVIRI instrument, this band will be used for upper-level tropospheric water vapor tracking, jet stream identification, hurricane track forecasting, mid-latitude storm forecasting, severe weather analysis, and for estimating upper level moisture.

3.11 7.0 μm

Based on the current GOES Sounder band 11 and the MSG/ SEVIRI instrument, this band will be used for mid-level tropospheric water vapor tracking, jet stream identification, hurricane track forecasting, mid-latitude storm forecasting, severe weather analysis, and for estimating upper level moisture.

3.12 7.4 μm

Based on the current GOES Sounder band 12, this band will provide flow information for the mid/lower levels of the atmosphere. It can also identify jet streaks. This band may help with volcanic plumes, especially if centered on 7.3 um.

3.13 8.5 μm

The 8.5 μm band, in conjunction with the 11.2 μm band, will enable detection of volcanic dust clouds containing sulfuric acid aerosols (Realmuto et al. 1997; Baran et al. 1993; Ackerman and Strabala 1994).

In addition, the 8.5 μm band can be combined with the 11.2 and 12.3 μm bands to derive cloud phase (Strabala et al. 1994). This determination of the microphysical properties of clouds includes a more accurate and consistent delineation of ice clouds from water clouds during the day or night.

Other uses of the 8.5 μm band include thin cirrus detection, in conjunction with the11 μm band (to improve other products by reducing cloud contamination), and a better atmospheric correction in relatively dry atmospheres (to improve SST). Surface properties can also be observed in conjunction with the 10.35 μm channel. The MSG carries a similar channel (8.5 to 8.9 μm) as well as MODIS and GLI.

3.14 9.7 μm

The inclusion of a thermal infrared ozone channel (9.7μm) on the GOES-R Imager would provide information both day and night about the real time dynamics of the atmosphere near the

tropopause on both high spatial and temporal resolutions. Significant wind shear, turbulence and tropopause folding occur in the middle latitudes, particularly during strongly baroclinic storms in the spring and fall. The 9.7 μm band may give some indications of clear-air turbulence. A 9.7μm channel on GOES ABI would also provide a good complement to a similar channel on Meteosat Second Generation, as part of a global observing system.

3.15 10.35 μm

The 10.35 μm band will help to derive low-level moisture, cloud particle size and surface properties. Chung et al. (2000) showed how the 10 - 11 μm region is important for determining particle sizes of ice clouds.

3.16 11.2 μm

The longwave infrared window (11.2 μm) band will provide day/night cloud analyses for general forecasting and broadcasting applications, precipitation estimates (Vicente et al. 1998), severe weather analyses, cloud drift winds (Velden et al. 1998a); hurricane strength (Velden et al. 1998b) and track analyses, cloud top heights, volcanic ash detection (Prata 1989), fog detection (in multi-band products) (Lee et al. 1997), winter storm monitoring, and cloud phase/particle size estimates (in multi-band products).

3.17 12.3 μm

The 12.3 μm band will offer nearly continuous cloud monitoring for numerous applications including: low-level moisture determinations; volcanic ash identification detection (Davies and Rose 1998); Sea Surface Temperature measurements (Wu et al. 1999) and cloud particle size (in multi-band products). It has been shown that mid-level dust amounts (within the Saharan Air Layer) can play a role in the lack of hurricane intensification in the Atlantic basin (Dunion and Velden 2001).

3.18 13.3 μm

The 13.3 μm band will be used for cloud top height assignments for cloud-drift winds, cloud products for ASOS supplement (Schreiner et al. 1993; Wylie and Menzel 1999), tropopause delineation, and estimating cloud opacity. These cloud products will be further improved by combining the data with high-spectral resolution sounder data.

Table 1 is a listing of the proposed 18 bands of the ABI. The “yellow-shaded ” bands correspond to similar bands on the current GOES imager. The “green-shaded” bands correspond to similar bands on the current Sounder or the MSG. The “magenta” bands are similar to bands on the MODIS or potential bands for the MTG (METEOSAT Third Generation). The bands are listed in order of increasing wavelength.

Band No.	Wavelength Microns	Bandpass microns	Primary Purpose
1	**0.47**	0.45-0.49	Daytime aerosol-on-land/coastal water mapping, vis.
2	**0.555**	0.545-0.565	Daytime "green" for true color, haze, smoke, etc
3	**0.64**	0.59-0.69	Daytime clouds fog, insolation, winds
4	**0.86**	0.84-0.88	Daytime vegetation & aerosol-on-water, winds
5	**1.38**	1.365-1.395	Daytime cirrus cloud
6	**1.61**	1.58-1.64	Daytime cloud water, snow
7	**2.26**	2.235 - 2.285	Daytime land/cloud properties, particle size, vegetation
8	**3.7**	3.61 - 3.79	Cloud properties and screening, hot spot detection, moisture
9	**3.90**	3.80-4.00	sfc. & cloud/fog at night, fire
10	**6.15**	5.7-6.6	High-level water, flow
11	**7.0**	6.8-7.2	mid-level water, flow
12	**7.4**	7.3-7.5	Lower-level water & SO2
13	**8.5**	8.3-8.7	total water for stability, cloud phase, dust, SO2
14	**9.7**	9.6-9.8	total ozone, turbulence, winds
15	**10.35**	10.1-10.6	sfc. & cloud, ice particle size
16	**11.2**	10.8-11.6	total water for SST, clouds, rainfall
17	**12.3**	11.8-12.8	total water & ash, SST
18	**13.3**	13.0-13.6	air temp & cloud heights and amounts

Partial Product list	Primary ABI Band(s)	Secondary ABI Band(s)	ABS/(HES)
aircraft icing threat	3.9. 8.5, 12.2	0.64, 11.2,	Yes.
atmospheric aerosols/dust	0.47, 8.5, 12.2, 2.2	0.55, 0.64, 0.86, 1.6, 11.2	
clear sky masks (Imager)	0.64,1.38,8.5,11.2,12.2	0.47,0.86,8.5,13.3	
cloud climatology	0.64, 1.38, 3.9, 11.2, 13.3	0.47	Yes.
cloud imagery	0.64, 1.38, 3.9, 11.2, 13.3	3.7	Yes.
cloud base/layer depth	*hyper-spectral imager?*		
cloud layers	0.64, 1.38, 3.9, 11.2, 13.3		Maybe
cloud liquid water	0.64	1.6, 2.2, 3.7	
cloud optical depth	0.64, 1.6	0.86	
cloud particle size	0.64,10.35	1.61, 11.2, 2.2	
cloud phase	1.6, 8.5	11.2, 2.2	Yes.
cloud top info	8.5, 13.3	11.2, 12.2	Yes.
Convection (and initiation)	0.64, 11.2, 6.15	7, 13.3	Yes.
Enhanced "V" detection	11.2	1.6, 6.15, 8.5	
fires (detection+information)	3.9, 11.2	0.64 12.2. 2.2, 3.7	
fire burn scars	0.86	0.64	
Hurricane intensity	11.2	0.64, 3.9, 6.15, 8.5, 12.2	Yes.
Insolation	0.64	0.47,0.56	
land surface temperature	11.2, 12.3	8.5	Yes.
low cloud and fog	3.9, 11.2	0.64, 1.61, 3.7	
Probability of rainfall	8.5, 11.2, 12.2, 13.3	0.64, 6.15	
rainfall rate/QPE	8.5, 11.2, 12.2, 13.3	0.64, 6.15	
derived motion (IR)	3.9, 11.2	9.7, 13.3	
derived motion (VIS)	0.64	11.2, 13.3	
derived motion (WV)	6.15, 7	11.2, 13.3	
sea ice products	0.64	11.2, 12.3	
Sea surface temperature	3.9, 11.2, 12.3	8.5	Yes.
Smoke	0.47, 0.64	0.56	
snow age		3.7, 3.9?	
snow detection (cover)	1.61	0.64	
snow rate			
SO2 concentration	8.5	7.4, 11.2, 9.6	
surface pressure	0.47?		
surface emmissivity			Yes.
surface properties	8.5, 10.35	11.2	Yes.
Suspended sediment	0.64	0.47, 0.55	
total ozone	9.6	11.2	Yes.
true color product	0.47,0.56, 0.64	0.86, 11.2	
Turbulence	6.15, 7, 9.6	11.2, 13.3	Maybe
under (ocean) surface features		0.47,0.56, 0.64?	
Vegetation index/fire potential	0.86	0.64	
Volcanic ash product	0.64, 3.9, 8.5, 12.3	11.2	Yes

Table 2 is a listing of selected imager products and the primary and secondary bands to compute those products. This is not an exhaustive list. ABS/HES refers to a potential product from the combined imager/sounder system.

Simulated GOES Advanced Baseline Imager examples will be shown for the bands in the visible, near infrared and infrared (IR) regions. Examples of ice and water clouds, fires and clear skies will be shown. The visible/near IR bands will be spectrally simulated from aircraft data--the NASA AVIRIS (Airborne Visible InfraRed Imaging Spectrometer). The AVIRIS is a high-spectral sensor with approximately 200 bands between 0.4 and 2.4 μm. The advantage of using hyperspectral data to simulate broadband channels is that any spectral response can be applied to test sensitivities. A tool to apply various spectral response functions to these AVIRIS data was used to simulate each visible/nearIR ABI band (Griffin 2003). The proposed spectral widths of certain bands were also investigated and realistic meteorological scenes were used. MODIS (MODerate-resolution Imaging Spectroradiometer) data will be used for the IR simulations.

4. SUMMARY

The ABI represents an exciting expansion in geostationary remote sensing capabilities. The ABI addresses the needs of the National Weather Service (and others) by increasing spatial resolution (to better depict a wider range of phenomena), by scanning faster (to improve temporal sampling and to scan additional regions) and by adding spectral bands (to enable new and improved products). Every product that is being produced from the current GOES Imager will be improved with data from the ABI. Furthermore, new products will be possible.

Of course the ABI will not be operating alone. Where appropriate, products will be produced in concert with the GOES-R high-spectral resolution sounder, for example, when generating cloud heights (Li et al. 2001). Also, the GOES system complements the polar systems and the entire Global Observing System (GOS).

The next generation METEOSAT (launched in 2002) has 12 bands, including two water vapor bands centered at 6.2 and 7.3 μm (Woick et al. 1997; Schmetz et al. 1998; Schmetz et al. 2002). Preliminary thoughts concerning the METEOSAT Third Generation satellite call for an imager with approximately 16 to 18 bands.

5. ACKNOWLEDGMENTS

The authors would like to thank a host of CIMSS and NESDIS scientists that contributed to this report.

6. REFERENCES

Ackerman, S. A., and H. Chung, 1992: Radiative effects of airborne dust on regional energy budgets at the top of the atmosphere. *J. Atmos. Sci.*, **31**, 223–236.

Ackerman, S. A., 1996: Global satellite observations of negative brightness temperature differences between 11 and 6.7 μm. *J. Atmos. Sci.*, **53**, 2803–2812.

Ackerman, S. A., K. I. Strabala, W. P. Menzel, R. A. Frey, C. C. Moeller, and L. E. Gumley, 1998: Discriminating clear sky from clouds with MODIS. *J. Geophys. Res*., **103**, 32141-32157.

Aquirre-Gomez, R., 2000: Detection of total suspended sediments in the North Sea using AVHRR and ship data. *Int. J. Remote Sensing*, **21**, 1583-1596.

Ba, M., and A. Gruber, 2001: GOES Multispectral Rainfall Algorithm (GMSRA). *J. Appl. Meteor*., in press.

Barton, I. J., A. J. Prata, I. G. Watterson, and S. A. Young, 1992: Identification of the Mount Hudson volcanic cloud over SE Australia. *Geophys. Res. Lett.*, **19**, 1211-1214.

Bayler, G. M., R. M. Aune, and W. H. Raymond, 2001: NWP cloud initialization using GOES sounder data and improved modeling of non-precipitating clouds. *Mon. Wea. Rev*., **128**, 3911-3920.

Baum, B. A., P. F. Soulen, K. I. Strabala, M. D. King, S. A. Ackerman,W. P. Menzel, and P. Yang, 2000: Remote sensing of cloud properties using MODIS Airborne Simulator imagery during SUCCESS. II. Cloud thermodynamic phase. *J. Geophys. Res.*, 105, 11,781-11,792.

Bosart, L. F., C. S. Velden, W. E. Bracken, J. Molinari, and P. G. Black, 2000: Environmental influences on the rapid intensification of Hurricane Opal (1995) over the Gulf of Mexico. *Mon. Wea. Rev.*, **128**, 322–352.

Casadevall, T.J., 1992: Volcanic hazards and aviation safety: Lessons of the past decade. *FAA Aviation Safety Journal*, 2 (3), 1-11.

Chung S., S. Ackerman, and P. F. van Delst, 2000: Model calculations and interferometer measurements of ice-cloud characteristics. *J. Appl. Met*., **39**, 634-644.

Davies, M. A., and W. I. Rose, 1998: Evaluating GOES imagery for volcanic cloud observations at the Soufriere Hills volcano, Montserrat. *Amer. Geophys. Union Proc*., in press.

Diak, G. R., M. C. Anderson, W. L. Bland, J. M. Norman, J. M. Mecikalski, and R. A. Aune, 1998: Agricultural management decision aids driven by real time satellite data. *Bull. Amer. Meteor. Soc*., **79**, 1345-1355.

Dostalek, J. F., J. F. Weaver, J. F. W. Purdom, and K. Y. Winston, 1997: PICTURE OF THE QUARTER: Nighttime Detection of Low-Level Thunderstorm Outflow Using a GOES Multispectral Image Product. *Weather and Forecasting*, **12**, 947–950.

Dunion J. P. and C. S. Velden, 2001: Satellite Applications for Tropical Wave/Tropical Cyclone Tracking. Preprints, *11th Conf. on Satellite Meteorology and Oceanography*, Madison, WI, Amer. Meteor. Soc., 314-317.

Ellrod, G. P., 1996: The use of GOES-8 multispectral imagery for the detection of aircraft icing regions. Preprints, *8th Conf. on Satellite Meteorology and Oceanography*, Atlanta, GA, Amer. Meteor. Soc., 168-171.

Ellrod, G. P., 2001: Loss of the 12.0 mm "split window" band on GOES-M: Impacts on volcanic ash detection. Preprints, *11th Conf. on Satellite Meteorology and Oceanography*, Madison, WI, Amer. Meteor. Soc., 61-64.

Ellrod, G. P., R. V. Achutuni, J. M. Daniels, E. M. Prins, and J. P. Nelson III, 1998: An assessment of GOES-8 Imager data quality. *Bull. Amer. Meteor. Soc*., **79**, 2509-2526.

Frey, R. A., B. A. Baum, W. P. Menzel, S. A. Ackerman, C. C. Moeller, and J. D. Spinhime, 1999: A comparison of cloud top heights computed from airborne LIDAR and MAS radiance data using CO_2-slicing, *J. Geophys. Res.*, **104**, 24,547-24,555.

Goerss, J. S., C. S. Velden, and J. D. Hawkins, 1998: The impact of multispectral GOES-8 wind information on Atlantic Tropical Cyclone track forecasts in 1995. Part II: NOGAPS Forecasts. *Mon. Wea. Rev*, **126**, 1219–1227.

Griffin, M. K., 2003: A Hyperspectral Adaptive Band Simulator Tool (AHABS) for Simulation of Multispectral Imagery. Preprints, *12th Conf. on Satellite Meteorology and Oceanography*, Long Beach, CA, Amer. Meteor. Soc.,

Gurka J. J., and G. J. Dittburner, 2001: The next generation GOES instruments: status and potential impact. Preprints *5th Symposium on Integrated Observing Systems*, Albuquerque, NM., Amer. Meteor. Soc.

Hayden, C. M., G. S. Wade, and T. J. Schmit, 1996: Derived product imagery from GOES-8. *J. Appl. Meteor*., **35**, 153-162.

Hillger, D. W., 1996: Meteorological features from principal component image transformation of GOES imagery, Proceedings, *GOES-8 and Beyond*, Intl. Soc. Optical Engineering, Denver, CO, 111-121.

Hillger, D. W., and J. Clark, 2002: Principal Component Image Analysis of MODIS for Volcanic Ash, Part-2: Simulation of Current GOES and GOES-M Imagers. Accepted by *J. Appl. Meteor.*

Hutchison, K. D., 1999: Application of AVHRR/3 imagery for improved detection of thin cirrus clouds and specification of cloud-top phase. *J. Atmos. Oceanic Tech*., **16**, 1885-1899.

Kim, D., and S. G. Benjamin, 2000: Assimilation of cloud-top pressure derived from GOES sounder data into MAPS/RUC. Preprints. *10th Conf. on Satellite Meteorology and Oceanography*, Long Beach, CA, Amer. Meteor. Soc., 110-113.

Lee, T. F., F. J. Turk, and K.Richardson, 1997: Stratus and Fog Products Using GOES-8–9 3.9-μm Data. *Wea. Forecasting*, **12**, 664–677.

Li, J., C. C. Schmidt, J. P. Nelson III, T. J. Schmit, and W. P. Menzel, 2001: Estimation of total atmospheric ozone from GOES sounder

radiances with high temporal resolution. *J. Atmos. Oceanic Technol.*, **18**, 157-168.

Li, J., W. P. Menzel, and A. J. Schreiner, 2001: Variational retrieval of cloud parameters from GOES sounder longwave cloudy radiance measurements. *J. Appl. Meteor*., **40**, 312-330.

Li, J., T. J. Schmit, and W. P. Menzel, 2002, Advanced Baseline Sounder (ABS) for future Geostationary Operational Environmental Satellites (GOES-R and beyond)", Proceedings of SPIE, *Applications with Weather Satellites*, Hangzhou, China,

Li, J., W. P. Menzel, Z. Yang, R. A. Frey, and S. A. Ackerman, 2002: High-spectral resolution surface and cloud type classification from MODIS multi-spectral band measurements. Submitted to *J. Appl. Meteor.*

Menzel, W. P., and J. F. W. Purdom, 1994: Introducing GOES-I: The first of a new generation of geostationary operational environmental satellites. *Bull. Amer. Meteor. Soc*., **75**, 757-781.

Moeller, C. C., S. A. Ackerman, K. I. Strabala, W. P. Menzel, and W. L. Smith, 1996: Negative 11 micron minus 12 micron brightness temperature differences: a second look. *8th Conf. on Satellite Meteorology and Oceanography*, Atlanta, GA, Amer. Meteor. Soc. 313-316.

Moody, J. L., A. J. Wimmers, and J. C. Davenport, 1999: Remotely sensed specific humidity: development of a derived product from the GOES Imager channel 3. G*eo. Phys. Let*., **26**, 59-62.

Mosher, F. R., 2001: A Satellite Diagnostic of Global Convection. Preprints, *11th Conf. on Satellite Meteorology and Oceanography*, Madison, WI, Amer. Meteor. Soc., 416-419.

Nieman, S. J., J. Schmetz, and W. P. Menzel, 1993: A comparison of several techniques to assign heights to cloud tracers. *J. Appl. Meteor.*, **32**, 1559-1568.

Prata, A. J., 1989: Observations of volcanic ash clouds in the 10-12 μm window using AVHRR/2 data. *Int. J. Remote Sens*., **10**, 751-761.

Prins, E. M., J. M. Feltz, W. P. Menzel, and D. E. Ward, 1998: An overview of GOES-8 diurnal fire and smoke results for SCAR-B and 1995 fire season in South America. *J. Geophysical Res*., **103**, 31821-31835.

Realmuto, V. J., A. J. Sutton, and T. Elias, 1997: Multispectral thermal infrared mapping of sulfur dioxide plumes: A case study from the East Rift Zone of Kilauea Volcano, Hawaii. *J. Geophys. Res*., **102**, 15,057-15,072.

Schmit, T. J., E. M. Prins, A. J. Schreiner, and J. J. Gurka, 2001: Introducing the GOES-M imager. Accepted by Nat. Wea. Assoc. Digest. Volume 25 Nos 3,4.

Schrab K. J., 2000: The use of AWIPS to display and analyze satellite data. Preprints, *10th Conf. on Satellite Meteorology and Oceanography*, Long Beach, CA, Amer. Meteor. Soc., 36-39.

Schreiner, A. J., D. A. Unger, W. P. Menzel, G. P. Ellrod, K. I. Strabala, and J. L. Pellett, 1993: A comparison of ground and satellite observations of cloud cover. *Bull. Amer. Meteor. Soc*., **74**, 1851-1861.

Schreiner, A. J., and T. J. Schmit, 2001: Derived cloud products from the GOES-M Imager. *11th Conf. on Satellite Meteorology and Oceanography*, , Madison, WI, Amer. Meteor. Soc., 420-423.

Schreiner, A. J., T. J. Schmit, and W. P. Menzel, 2001: Trends and observations of clouds based on GOES sounder data. Accepted by *J. Geophysical Res. --Atmospheres*.

Seki, M. P., J. J. Polovina, R. E. Brainard, R. R. Bidgare, C. L. Leonard, and D. G. Foley, 2001: Biological enchancement at cyclonic eddies tracked with GOES thermal imagery in Hawaiian waters. *Geophysical Research Letters*, **28** (8), 1583.

Schmetz, J., H. Woick, S. Tjemkes, and J. Rattenborg, 1998: From Meteosat to Meteosat Second Generation. Proceedings, *9th Conf. on Satellite Meteorology and Oceanography*, Paris, France, Amer. Meteor. Soc., 335-338.

Schmetz, J., P. Pili, S. Tjemkes, D. Just, J. Kerkmann, S. Rota, and A. Ratier, 2002: An Introduction to Meteosat Second Generation (MSG). *Bull. Amer. Meteor. Soc*., **83**, 977–992.

Soden, B. J., and F. P. Bretherton, 1993: Upper tropospheric relative humidity from the GOES 6.7 μm channel: Method and climatology for July 1987. *J. Geophys. Res.*, **98**, 16669-16688.

Strabala, K. I., S. A. Ackerman, and W. P. Menzel, 1994: Cloud properties inferred from 8-12 μm data. *J. Appl. Meteor*, **33**, 212-229.

Velden, C. S., C. M. Hayden, S. J. Nieman, W. P. Menzel, S. Wanzong, and J. S. Goerss, 1997: Upper-tropospheric winds derived from geostationary satellite water vapor observations. *Bull. Amer. Meteor. Soc.*, **78** , 173-173.

Velden, C. S., T. L. Olander, and R. M. Zehr, 1998a: Development of an objective scheme to estimate tropical cyclone intensity from digital geostationary satellite infrared imagery. *Wea. Forecasting*, **13** , 172–186.

Velden, C. S., T. L. Olander, and S. Wanzong, 1998b: The impact of multispectral GOES-8 wind information on Atlantic tropical cyclone track forecasts in 1995. Part I: dataset methodology, description, and case analysis. *Mon. Wea. Rev.*, **126**, 1202–1218.

Vicente, G. A., R. A. Scofield, and W. P. Menzel, 1998: The operational GOES infrared rainfall estimation technique, *Bull. Amer. Meteor. Soc.*, **79** , 1883–1898.

Weldon, R. B, and S. J. Holmes, 1991: Water vapor imagery -- interpretation and applications to weather analysis and forecasting. NOAA Technical Report NESDIS 57.

Woick, H., J. Schmetz, and S. Tjemkes, 1997: An introduction to Meteosat Second Generation imagery and products. *1997 Meteorological Data Users' Conference*, Brussels, Belgium.

Wu, Xiangqian, W. P. Menzel, and G. S. Wade, 1999: Estimation of sea surface temperatures using GOES-8/9 radiance measurements. *Bull. Amer. Meteor. Soc.*, **80** , 1127-1138.

Wylie, D. P., W. P. Menzel, H. M. Woolf, and K. I. Strabala, 1994: Four years of global cirrus cloud statistics using HIRS. *J. Climate*, **7**, 1972-1986.

Wylie, D. P., and P. H. Wang, 1997: Comparison of cloud frequency data for the High Resolution Infrared Radiometer Sounder and the Stratospheric Aerosol and Gas Experiment II. *J. Geophys. Res.*, **102** (29), 29,893-29,900.

Wylie, D. P., and W. P. Menzel, 1999: Eight years of high cloud statistics using HIRS. *J. Climate*, **12**, 170-184.